Earth and Space Science

TECHNICAL REPORTS: METHODS
10.1029/2019EA000566

Evaluation of a Microwave Emissivity Module for Desert Regions With CMEM

M. Lange[1] and P. de Rosnay[2]

[1]Deutscher Wetterdienst, Offenbach, Germany, [2]European Centre for Medium-Range Weather Forecasts (ECMWF), Reading, UK

Key Points:
- Use of satellite derived soil moisture in NWP
- Advancing soil moisture Assimilation using passive L-Band surface Emission
- Demonstration of impact on simulated brightness temperatures with CMEM against SMOS observations

Supporting Information:
- Supporting Information S1

Correspondence to:
M. Lange,
martin.lange@dwd.de

Citation:
Lange, M., & de Rosnay, P. (2019). Evaluation of a microwave emissivity module for desert regions with CMEM. *Earth and Space Science*, *6*, 1787–1795. https://doi.org/10.1029/2019EA000566

Received 25 JAN 2019
Accepted 9 JUL 2019
Accepted article online 16 JUL 2019
Published online 30 SEP 2019

Abstract To overcome deficiencies of current state-of-the-art L-band microwave emission models a microwave emissivity parameterization for desert regions, as derived by Grody and Weng (2008) using dense media theory, has been implemented in European Centre for Medium-Range Weather Forecasts' Community Microwave Emission Modeling platform (CMEM). Simulations of L-Band brightness temperatures were conducted over Africa for 2013 using the default CMEM parameterization of the soil dielectric constant from Wang and Schmugge, and using the desert emissivity parameterization from Grody and Weng. Results are evaluated against Soil Moisture and Ocean Salinity mission data. The Grody and Weng parameterization shows clear improvements over dry soil in arid areas with reduced bias and root-mean-square deviations at both polarizations. However deficiencies for semi-arid areas, where the bare soil model of Wang and Schmugge shows best results in rainy conditions, suggest that hybrid implementation combining soil dielectric and desert emissivity models should be investigated for global scale applications.

1. Introduction

The Community Microwave Emission Modeling platform (CMEM) was developed by the European Centre for Medium-Range Weather Forecasts (ECMWF) for simulations of brightness temperature in the microwave region from 1–20 GHz (de Rosnay et al., 2009; Holmes et al., 2008). It was validated in a number of studies using field campaigns data (Parrens et al., 2014; Sabater et al., 2011) as well as satellite data and model intercomparison studies (de Rosnay et al., 2009; Drusch et al., 2009; Tian et al., 2015). At ECMWF it is used as forward model in L-band to use top of atmosphere (TOA) brightness temperature observations from the SMOS (Soil Moisture and Ocean Salinity) and the SMAP (Soil Moisture Active Passive) satellites (Entekhabi et al., 2010; Kerr et al., 2001) to improve soil water content and near-surface weather forecasts.

CMEM takes into account subgrid-scale variability, so that it can simulate brightness temperature for heterogeneous surface conditions as vegetated areas (Jackson & Schmugge, 1991; Pellarin et al., 2003; Wigneron et al., 2007) frozen soil, bare soil (Mironov et al., 2004a; Wang & Schmugge, 1980; Wilheit, 1978), and snow-covered surfaces. Details can be found in de Rosnay et al. (2009).

Emissivity of dry sandy soils, deserts, or snow surfaces is characterized by the scattering of closely spaced particles as derived from dense media theory (Tsang et al., 1985). However, the scattering effect of desert areas is not represented in current models such as CMEM or L-band Microwave Emission of the Biosphere (Wigneron et al., 2007). In these models, the soil emissivity for dry sand is treated as for bare soil, and it relies on dielectric mixing models, for example, the Wang snd Shmugge (1980, WS in the following), which is the default parameterization used in CMEM, or Mironov et al. (2004a) used in L-band Microwave Emission of the Biosphere or the Dobson et al. (1985) parameterization. In L-band wavelength is large compared to particle radius and scattering of electromagnetic radiation at neighboring particles can no longer be considered independently. Consequently, the far-field approximation is no longer valid. Grody and Weng (2008; for convenience GW in the following) calculated the emissivity for closely spaced particles using the two stream approximation for radiative transfer (Liou, 1980), which is more appropriate for dry and semiarid conditions. Due to the heterogeneous soil moisture conditions that vary in space and in time, both a specific desert emissivity model and dielectric mixing models are necessary to represent the range of soil emissivity variations.

This paper presents the implementation of the Grody and Weng (2008) parameterization in CMEM. Performances of CMEM using the GW and WS models is evaluated against SMOS L-band brightness temperature measurements for arid and semi arid conditions in Africa.

Section 2 describes the CMEM simulations and experimental setup as well as the SMOS brightness temperature data used in this paper. Results are presented in section 3, and they are discussed in section 4, which also concludes the paper.

2. Data and Methods

2.1. SMOS Data

The SMOS data set release v505 was used for evaluation of the model simulations. SMOS is European Space Agency's first polar orbiting mission to provide L-band (1.4 GHz) brightness temperatures, for soil moisture and ocean salinity measurements from space (Kerr et al., 2016). Observations from the 6:00 LST ascending path were selected for the evaluation, which provide the best conditions with respect to minimal daily ionospheric perturbations and moderate vertical surface soil moisture gradients. Near-surface soil moisture and its vertical gradient have a strong influence on the sensitivity of soil emissivity (Njoku & Entekhabi, 1996) and, therefore, may affect the quality of the retrieval. The same applies for the thermal profile, best estimates of effective temperature can be achieved with a low vertical resolution land surface model under homogeneous soil conditions.

Level 1 SMOS near-real time brightness temperature (TB) data were used for this study. The product was regridded to the ECMWF TL511 (40-km resolution) reduced Gaussian grid using a bilinear interpolation. A quality check included filtering out observations over snow-covered or frozen surfaces, using ERA-Interim information. SMOS data were also filtered for pixels indicated by the product quality flags to be outside the alias free field of view, with water fraction >5%, or affected by radio frequency interferences.

2.2. CMEM and Experimental Setup

TBs were simulated over North Africa with CMEM (de Rosnay et al., 2009) at ~40-km resolution (TL511), for the year 2013, for a time window covering 06 UTC ± 3 hr. CMEM input includes soil moisture and soil temperature, taken from the H-TESSEL land surface model simulations forced by ERA-Interim atmospheric forcing (Balsamo et al., 2015). So model soil moisture heavily depends on ERA-Interim precipitation, and possible biases are reflected in the model simulations. H-TESSEL represents soil moisture using four layers of 7, 21, 72 cm and 1.89 m from top to bottom. It uses the United Nations Food and Agriculture Organization (FAO) soil texture data base and the United States Geophysical Survey Global Land Cover Classification (GLCC) as described in Balsamo et al. (2015). CMEM simulations provides top of the atmosphere brightness temperature at H and V polarizations. Faraday rotation was applied to CMEM output as a postprocessing to account for ionospheric effects on the polarization of the signal. The obtained TBs are at xx and yy polarizations in the SMOS antenna frame, so they can be compared to the SMOS observations.

Two CMEM-simulations of brightness temperature are compared in this paper to show the performance of the different models for different soil conditions with main focus on dry conditions in desert regions:

a. is the reference experiment, using the dielectric mixing model from WS without any special treatment of deserts.
b. uses the Grody and Weng (2008) microwave emission parameterization applied for all soil types and conditions in the selected domain.

2.3. Validation Domain and Metrics

The study area is shown in Figure 1a (large box), covering a north African domain from 10° to 40° north in latitude and −20° to 45° in longitude. The Sahara desert is one of the largest areas on Earth with quasi-permanent dry conditions, so it is very relevant to evaluate the performance of the GW desert emissivity model. The evaluation metrics for land in the study area include bias, root-mean-square deviation (rmsd), standard deviation, and correlation statistics. Results are presented in 1° × 1° grid spacing using nearest neighbor interpolation, which represents the various soil and surface properties in the model domain. The reduced resolution allows for efficient experimentation and is justified by the homogeneous surface conditions. Figure 1a also illustrates the H-TESSEL volumetric soil water content of the top soil layer (0–7 cm) used as input of CMEM for 1 May 2013. Figure 1b shows the FAO soil sand fraction as reference to indicate regions where it is expected that the GW parameterization improves the simulation of the Ctrl run, since the

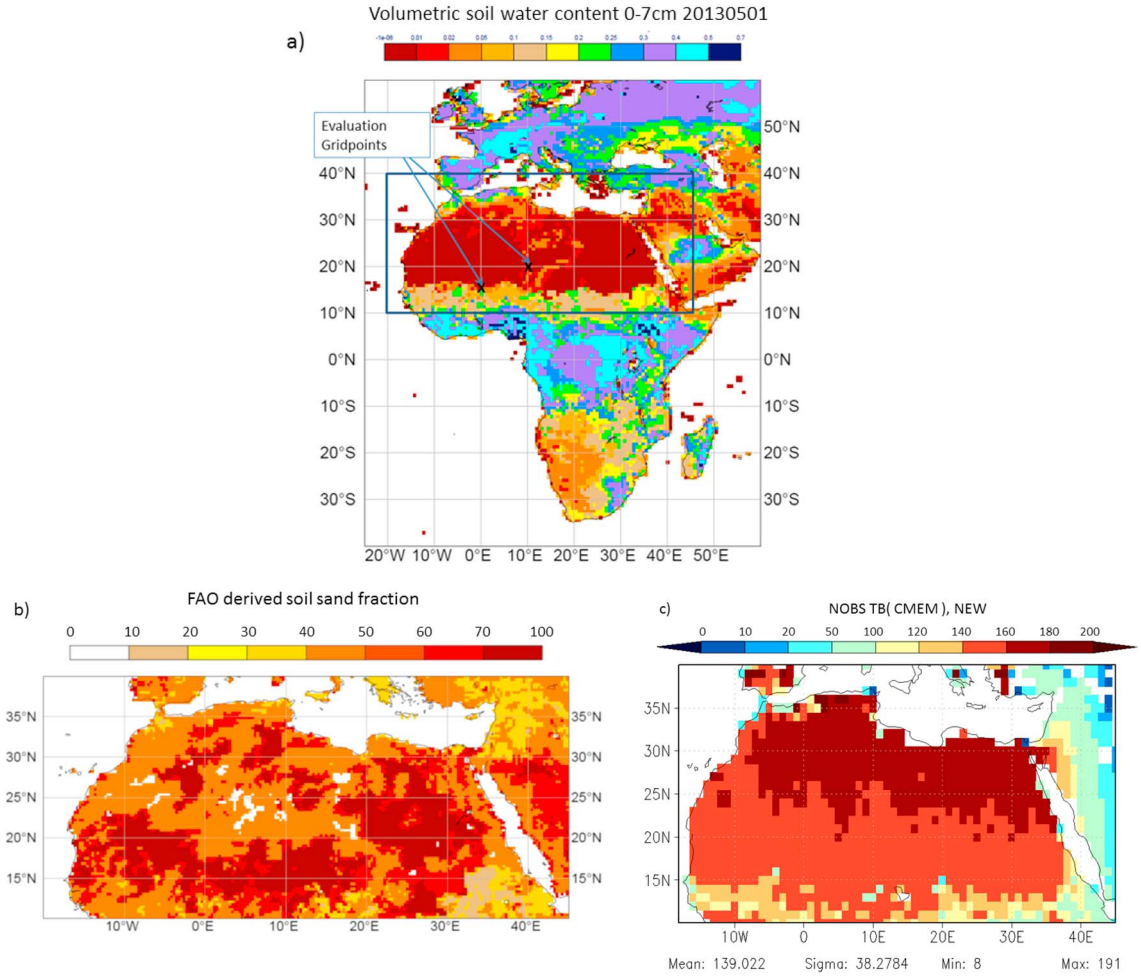

Figure 1. Panel (a) shows the study area (blue rectangle extends from southern Sahel and covers the Sahara desert region), with color shading showing model top layer (0–7 cm) soil moisture for 1 May 2013. Black crosses indicate grid points selected for time series comparison and validation of dielectric models in arid and semiarid conditions. Panel (b) shows the FAO-derived sand fraction used at ECMWF in H-TESSEL and in CMEM and panel (c) indicates the number of SMOS observations used in the statistics for evaluation of the new parameterization with CMEM. FAO = Food and Agriculture Organization; ECMWF = European Centre for Medium-Range Weather Forecasts; CMEM = Community Microwave Emission Modelling Platform; TB = brightness temperatures.

underlying theory is based on the coarse grain soil texture. This should reflect if the FAO sand classification corresponds to the respective soil dielectric properties.

For the studied time window of 06:00 UTC ± 3 hr, the 6:00 LST SMOS ascending path covers a region from the African west coast to the Arabian peninsula at 45° east with decreasing number of observations toward the eastern boundary as indicated in Figure 1c.

In addition to the regional scale analysis, local scale analysis is conducted at two local grid points to illustrate time series of SMOS and CMEM using different parameterization schemes. These two sites, indicated by black crosses on Figure 1a, are located in central Sahara and in north Sahel, are representative of desertic conditions with persistent dry conditions all the year (no rainfall season), and Sahelian conditions with a single short rainfall season leading to more contrasted annual cycles of soil moisture.

3. Results

3.1. Grid Point Evaluation

Figure 2 shows the time series of 1.4 GHz brightness temperature simulated with CMEM using the GW parameterization (New, green) and WS dielectric model (Ctrl, red), as well as the SMOS observations (black), at both xx (left) and yy (right) polarizations. The volumetric surface soil moisture content is indicated as

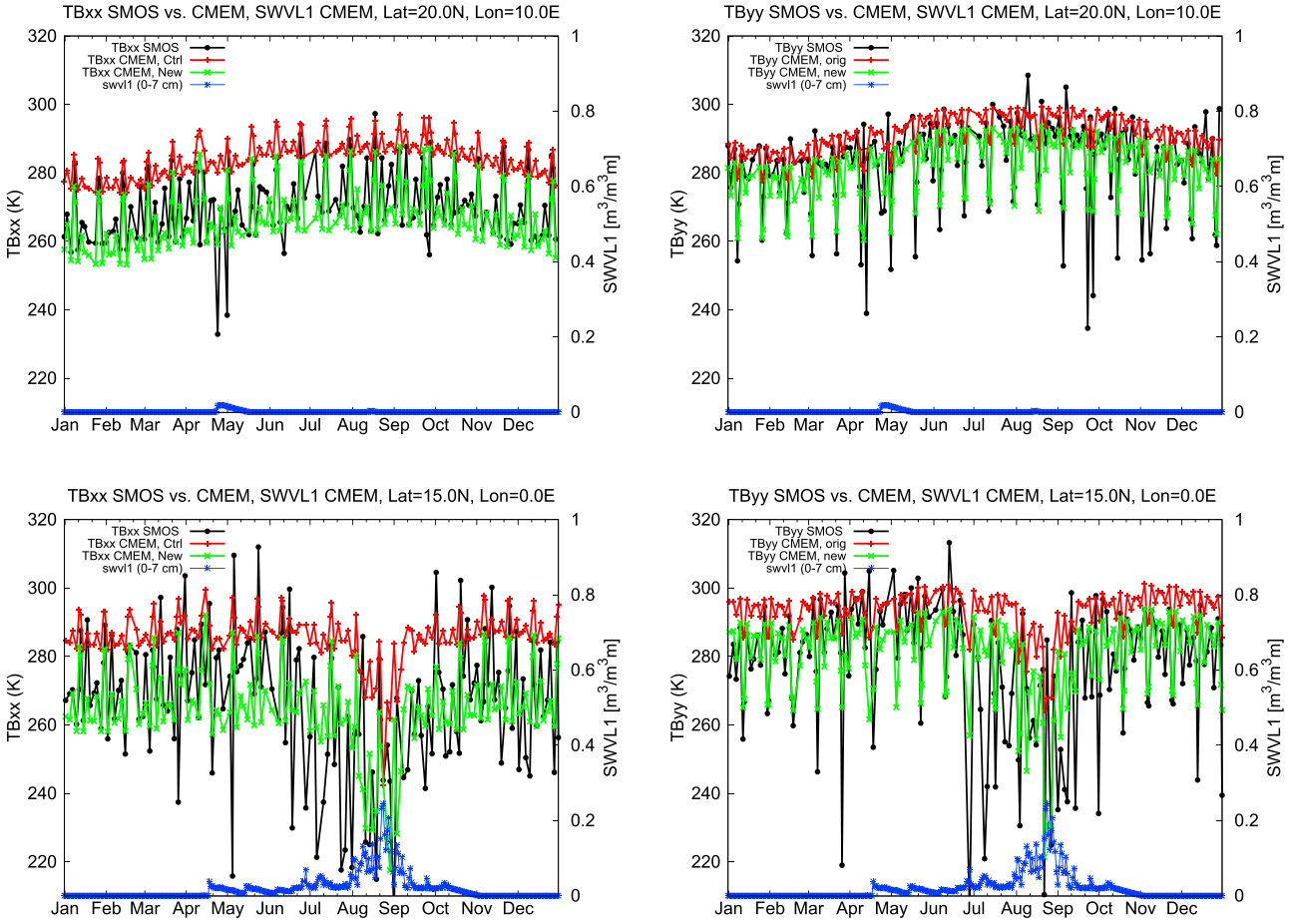

Figure 2. Simulated CMEM brightness temperatures in the SMOS reference frame at xx-polarization (left column) and yy-polarization (right column), for the Saharian site (top row) and the Sahelian site (bottom row), for the New simulation using GW (green), the Ctrl using WS (red), and SMOS observations (black). The blue line indicates volumetric soil water content in top model layer (0–7 cm), scaled on the right *y* axis. CMEM = Community Microwave Emission Modelling Platform; SMOS = Soil Moisture and Ocean Salinity; TB = brightness temperatures.

blue line with scaling on the right axis. Time series are presented for the Saharian and the Sahelian local sites indicated in Figure 1a.

Figure 2 shows that in dry conditions the GW parameterization (green line) generally improves the simulated TB against SMOS observations (black) when compared to the Ctrl using WS (red). In the Ctrl, simulated brightness temperatures with the WS dielectric model, show a positive bias (red line), larger at xx than at yy polarization. This bias, which mostly occurs in dry conditions, is reduced by more than 15 K at xx-polarization when the GW parameterization is used instead of WS (Figure 2, left column). The dynamic range is also better reproduced with larger amplitude for GW than with WS. In contrast, in relatively wet conditions, during the rain season, Figure 2 (bottom row) shows some clear differences in particular during the June to August period. Strong downward peaks that occur in SMOS TB are not captured by both simulations. In the dry period end of March a strong downward peak occurs, as typical for wet soil conditions, which is not present in the model simulations. The blue line indicates no increase of surface soil moisture so a possible explanation might be that ERA-Interim model forcing misses that precipitation event. Insufficient precipitation may also hold for the low variability during June to August. Earlier studies have reported that a slight underestimation in Sahel (Nkiaka et al., 2016) showed that in the Sudano-Sahel region, ERA-Interim precipitation tends to have a negative precipitation bias of the order of 6 mm/month and root-mean-square error of 2%, with overall lower bias and lower errors than the Climate Forecasting System Reanalysis (CFSR). Diallo et al. (2012) evaluated precipitation skills from ERA-Interim and seven regional climate models, against three different data sets (CRU, CMAP, GPCP) in West Africa. They showed that ERA-interim captures the spatial patterns and amount of precipitation although the area of intense precipitation is shifted southward.

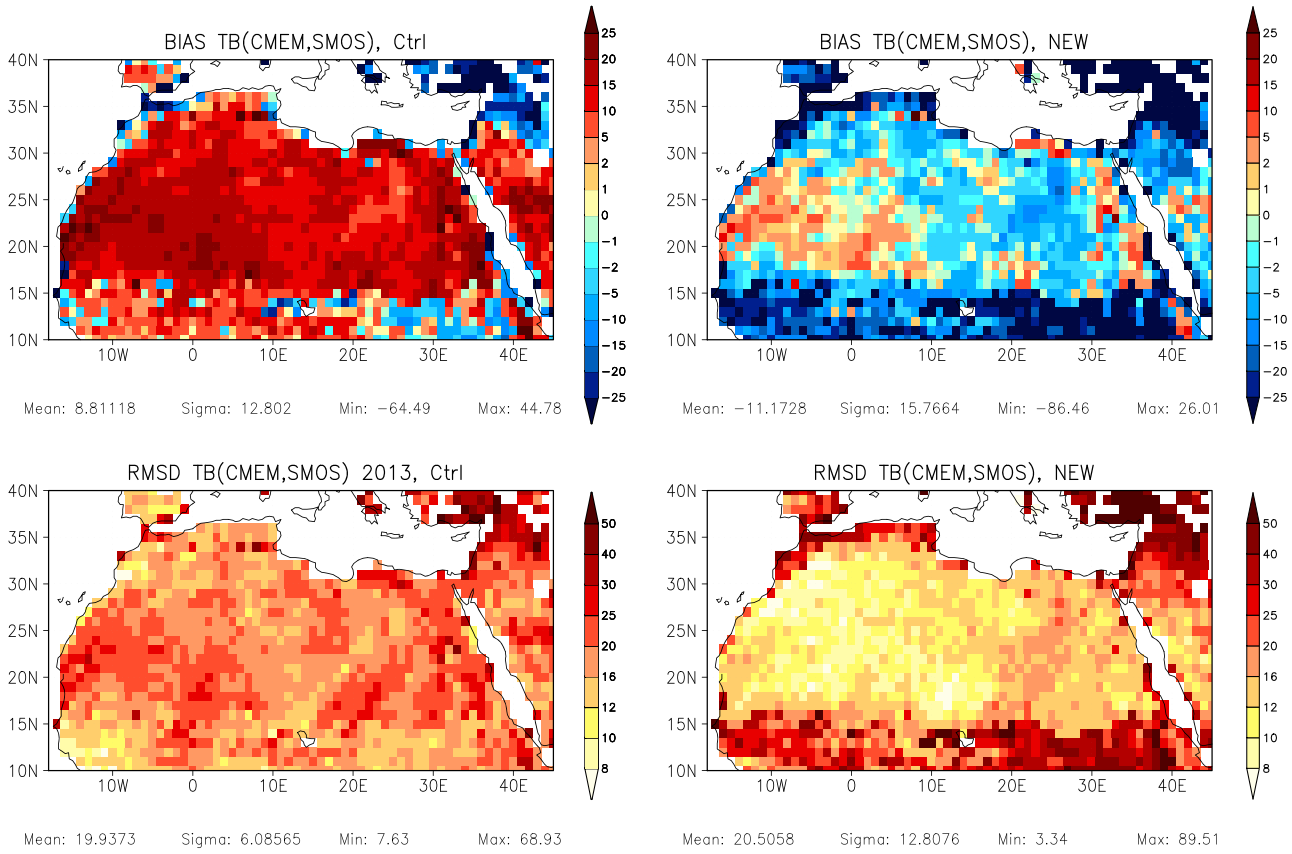

Figure 3. Annual mean bias and root-mean-square deviation (K) of CMEM brightness temperature for 2013 compared to SMOS observations in the validation domain. Left panels show results for the Ctrl experiment with the Wang and Schmugge scheme, the right panels show results for the New experiment using Grody and Weng parameterization. CMEM = Community Microwave Emission Modelling Platform; SMOS = Soil Moisture and Ocean Salinity; TB = brightness temperatures.

3.2. Evaluation of Sahara Domain

Figure 3 shows maps of annual mean bias and rmsd of TB for the Ctrl (WS) and New (GW) experiments. Results are presented on 1° × 1° grid spacing, obtained by NN interpolation, representing well the soil and surface conditions in the 40-km resolution model grid. As already shown for the two locations chosen for Figure 2, the WS scheme generally shows poor agreement with the SMOS TB in the arid Sahara desert region (illustrated in Figure 1 for one date), with warm positive biases around 15 to 20 K and 15 K on domain average.

An overall better agreement with the SMOS observations is obtained in the New experiment, using the GW parameterization, with a mean bias of −11 K for the study area. The annual mean bias remains mostly below 5 K for the dry grid points with volumetric soil water content below 1 m^3/m^3. For the Sahelian region, south of 15° north, a large cold bias below −20 K in the New experiment indicates that the GW parameterization is generally not able to reproduce the SMOS observations for nondesertic soil moisture conditions.

Maps of rmsd in the lower panels of Figure 3 confirm the overall improvement provided by the GW parameterization in desertic conditions, with much reduced rmsd values in the New experiment than in the Ctrl. The central part of Sahara is characterized by rmsd values lower than 10 K with GW (shown in yellow in Figure 3, bottom right), whereas values larger than 15 K are obtained with WS (reddish colors in Figure 3, bottom left).

Temporal Variability. To further evaluate the temporal variability of SMOS TB with the simulations unaffected from biases, Figure 4 shows annual mean standard deviation for SMOS TB and the Ctrl run and the differences between both experiments and SMOS. As found at local scale analysis, the amplitude observed for SMOS (top left) is not captured at all with the Ctrl run, which shows much smaller values in the central Sahara around 4–6 K, and in the northern part around 6–8 K, compared to 10–15 K or even higher

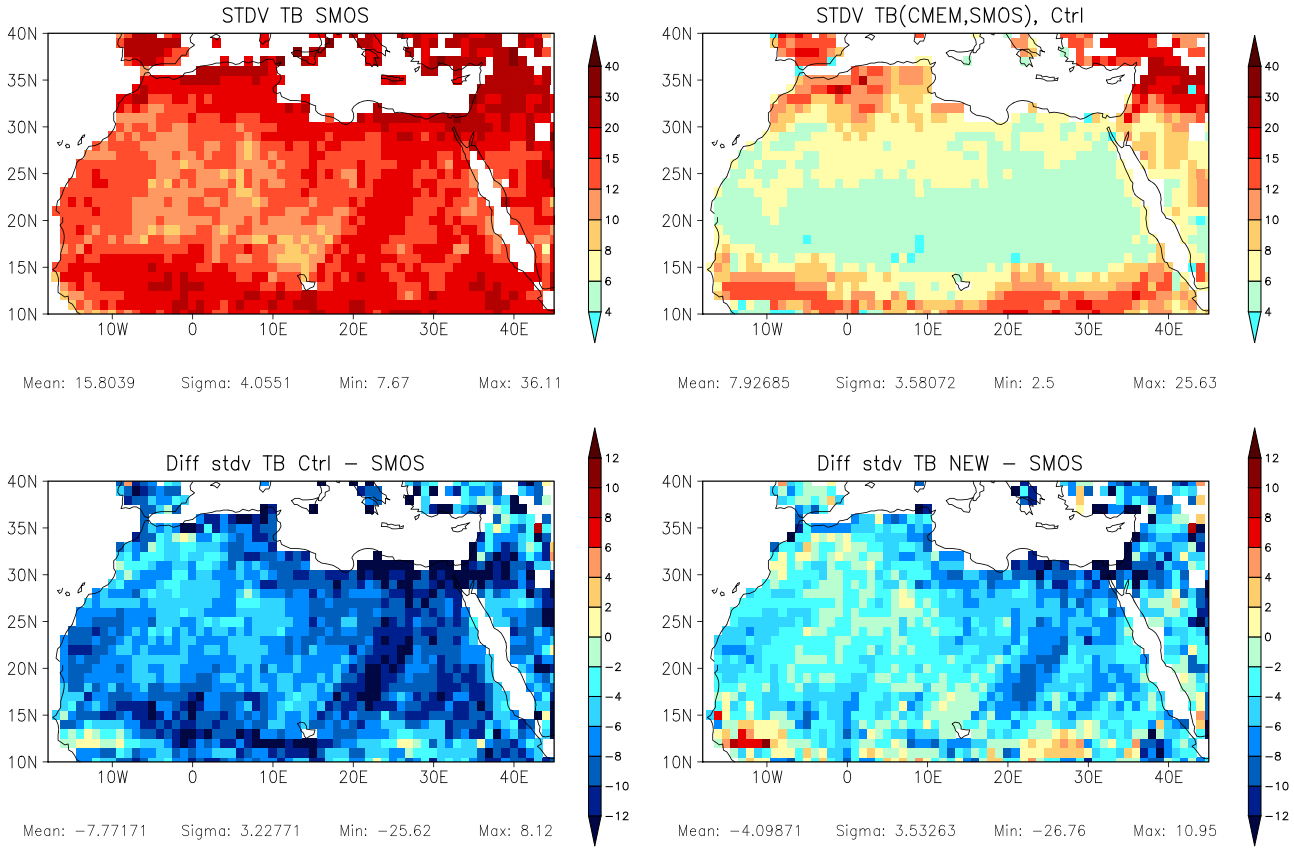

Figure 4. Maps of standard deviation for SMOS TB and the Ctrl experiment (top panels), and differences between CMEM simulations and SMOS TB (bottom panels). SMOS = Soil Moisture and Ocean Salinity; TB = brightness temperatures; CMEM = Community Microwave Emission Modelling Platform.

values for SMOS TB. The blue shading shown in the difference plots in the bottom panels reflects the clear improvement for the new GW parametrization that fits much better with a domain average of −4 K difference compared to −7.8 K for WS. For the Sahara region GW shows differences of standard deviation around −2 to −4 K whereas large regions show values below −6 K when WS is used.

Correlation Statistics. Figure 5 shows maps of annual correlation statistics, for 2013, between the SMOS observations and the Ctrl experiment and difference between correlation values obtained for the New and Ctrl experiments. The clear improvement obtained with GW in desertic areas for bias, rmsd, and standard deviation is not reflected in correlation statistics against SMOS data, as shown by the correlation difference

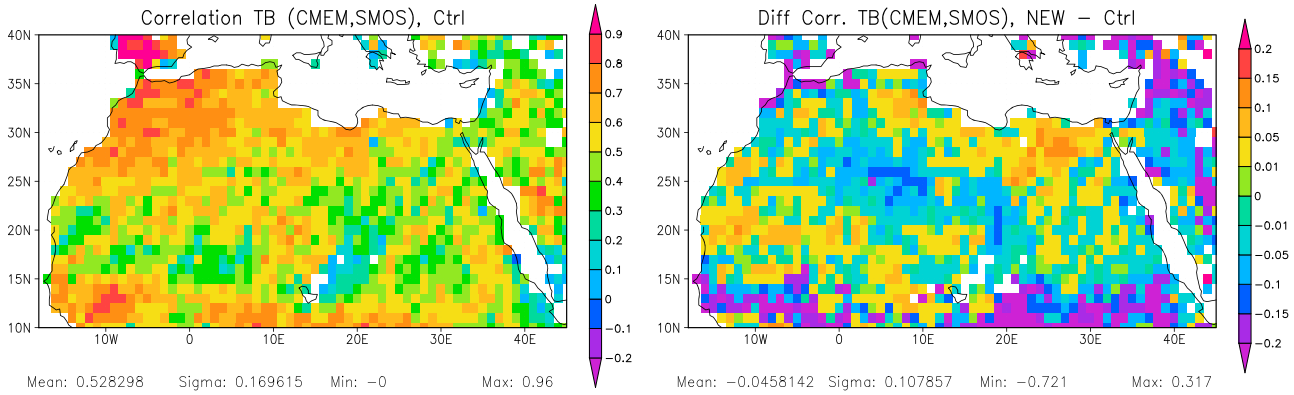

Figure 5. Maps of correlation statistics between SMOS and CMEM TB for the Ctrl experiment (left) and difference between New and Ctrl correlation with SMOS TB (right). SMOS = Soil Moisture and Ocean Salinity; TB = brightness temperatures; CMEM = Community Microwave Emission Modelling Platform.

Table 1
Domain Average Statistics for the Model Simulations Against SMOS Tb in a Subdomain With Desert Conditions

	Bias	rmsd	Diff. stdv	Corr
Ctrl	14.7 K	19.9 K	−7.8 K	0.54
New	-2.3 K	13.5 K	−4.5 K	0.53

Note. The latitude range is bounded by 20–30°N, the longitude range is preserved. Difference of standard deviation (Diff. stdv.) is calculated with respect to model-observation. SMOS = Soil Moisture and Ocean Salinity; rmsd = root-mean-square deviation.

map (right panel). This region is characterized by a very low annual variability, which makes it difficult to compute significant correlation statistics, leading to noisy differences.

The GW parameterization is based on scattering at closely spaced particles with particle radius small compared to the wavelength and considers coarse grain sand like soil texture. The FAO sand fraction, depicted in the right panel of Figure 1 shows this correspondence with the higher correlation for GW in the southwest and northeastern Sahara region, where sand fraction exceeds 70%. In the central Sahara and in the northern part of the Arabian peninsula, where sand fraction is below 50% and below 30%, respectively, the correlation for GW is smaller compared to WS. Thus, the GW parameterization is beneficial when both dry conditions and sandy soil texture dominate the regional soil properties; elsewhere the default WS parameterization should be applied. For the intermediate range, that is, mixed type of soil texture and moderate wet conditions, a combined approach should be the best option, which requires more investigation on blending strategy and on a proper bias correction.

Statistics are provided in Table 1 for a subdomain 20–30°N corresponding to desert conditions for which GW is relevant, showing a clear improvement compared to WS.

Bias correction applied to the microwave emission model parameterizations. CMEM forward model is used by the scientific community for data assimilation purposes (e.g., Muñoz Sabater et al., 2018, 2019). Data assimilation aims at correcting for the model random errors, so a bias correction is applied a priori to match the CDF of the model and observation mean and variances (Reichle & Koster, 2004).

To assess the performance in the data assimilation environment, a seasonal bias correction is applied to both the Ctrl and New experiments first guess departure statistics, following the approach of Reichle and Koster (2004) and Draper et al. (2012). The investigation shows that correlation differences between New and Ctrl after bias correction is mostly neutral with values of 0.53 and 0.57, Bias is almost removed from the time series, values are −0.003 K for New, and −0.048 K for Ctrl, and rmsd is reduced to 14 and 13.9 K, respectively. This indicates that both GW and WS perform similarly after bias correction and so, either can be used for data assimilation perspectives. The applicaton of the new parameterization in the desert region, however, would reduce the tuning effort for the determination of the bias correction coefficients.

4. Conclusions

This study shows a first evaluation of the microwave emissivity parameterization for dry soil conditions after GW, where scattering theory for dense media applies and present microwave emission models show large errors. Results from CMEM using the GW parameterization and the WS dielectric model are compared and evaluated against the SMOS measurements. The study focuses on the Sahara region using ECMWF's radiative transfer modeling environment CMEM by comparison with SMOS TB measurements for the 2013 period.

Results show that, compared to WS, the GW parameterization leads to simulated TB in better agreement with the SMOS data over most of the desert area. Mean annual bias is reduced from 15 K with WS to less than 5 K with GW at xx-polarization, and rmsd values are significantly reduced by more than 10 K over most of the study area. The reduction of the difference in standard deviation between simulations and SMOS from −7.8 to −4 K on domain average confirms that GW captures much better the variability of the SMOS signal than WS. Obviously, it is desired to use the best model to keep the tuning effort as small as possible. Therefore, the GW parameterization is recommended for the desert regions whereas the WS model is better suited for nondesertic areas. Correlation statistics show relatively small differences of using GW compared to WS due

to low temporal dynamics in this area, which makes correlation assessment less relevant than bias, rmsd, and standard deviation. For data assimilation perspectives, a bias correction, based on CDF-matching, was applied and first guess departure statistics were computed for both simulations. Results show neutral impact when either GW or the WS are used. So, a combined approach, using GW over deserts and WS elsewhere, should be considered to provide best overall agreement in terms of rmsd and bias, with smallest effort on tuning the bias correction coefficients.

Further investigation is recommended to explore methods to combine the two model approaches in a modular way so that the full range of soil moisture conditions, including desertic, semiarid, and wet conditions, can be represented in forward models. Good results for the GW parameterization under moderate wet conditions suggest a linear combination of GW parameterization and WS in the range 5–10%. For soil textures with small sand fraction the application of the GW model should be further quantitatively assessed.

Acknowledgments
The authors thank Yudong Tian for helping with the Grody and Weng code development in CMEM. They also thank the two reviewers for their helpful comments and suggestions. The data and software used to obtain the results are located at Hydroshare repository: Lange, M. 2019 mlange_pdrosnay_paper_ess_2019, HydroShare http://www.hydroshare.org/resource/b47fde6aea274ce0a8992a429e108644

References

Balsamo, G., Albergel, C., Beljaars, A., Boussetta, S., Cloke, H. L., Dee, D., et al. (2015). ERA-Interim/Land: A global land water resources dataset. *Hydrology and Earth System Sciences*, *19*, 389–407. https://doi.org/10.5194/hess-19-389-2015

de Rosnay, P., Drusch, M., Boone, A., Balsamo, G., Decharme, B., Harris, P., et al. (2009). The AMMA land surface model Intercomparison experiment coupled to the Community Microwave Emission Model: ALMIP-MEM. *Journal of Geophysical Research*, *114*, D05108. https://doi.org/10.1029/2008JD010724

Diallo, I., Sylla, M. B., Amadou, M. C., & Gaye T. (2012). Interannual variability of rainfall over the Sahel based on multiple regional climate models simulations. *Theoretical and Applied Climatology*, *113*, 351–362. https://doi.org/10.1007/s00704-012-0791-y

Dobson, M., Ulaby, F., Hallikainen, M., & El-Rayes, M. (1985). Microwave dielectric behavior of wet soil-part II: Dielectric mixing models (1985). *IEEE Transactions on Geoscience and Remote Sensing*, *38*, 1635–1643.

Draper, C., Reichle, R., De Lannoy, G., & Liu, Q. (2012). Assimilation of passive and active microwave soil moisture retrievals. *Geophysical Research Letters*, *39*, L04401. https://doi.org/10.1029/2011GL050655

Drusch, M., Holmes, T., de Rosnay, P., & Balsamo, G. (2009). Comparing ERA-40 based L-band brightness temperatures with Skylab observations: A calibration/validation study using the Community Microwave Emission Model. *Journal of Hydrometeorology*, *10*, 213. https://doi.org/10.1175/2008JHM964.1

Entekhabi, D., Njoku, EniG., O'Neill, P. E., Kellogg, K. H., Crow, W. T., Edelstein, W. N., et al. (2010). The Soil Moisture Active Passive (SMAP) mission. *Proceedings of the IEEE*, *98*(5), 704–716.

Grody, N. C., & Weng, F. (2008). Microwave emission and scattering from deserts: Theory compared with satellite measurements. *IEEE Transactions on Geoscience and Remote Sensing*, *46*, 361–375.

Holmes, T., Drusch, M., Wigneron; J. P., & de Jeu, R. (2008). A global simulation of microwave emission: Error structures based on output from ECMWF's operational integrated forecast system. *IEEE Transactions on Geoscience and Remote Sensing*, *46*(3), 846–856. https://doi.org/10.1109/TGRS.2007.914798

Jackson, T., & Schmugge, T. (1991). Vegetation effects on the microwave emission of soils. *Remote Sensing of Environment*, *36*, 203–212.

Kerr, Y., Reul, N., Martín-Neira, M., Drusch, M., Alvera-Azcarate, A., Wigneron, J.-P., & Mecklenburg, S. (2016). ESA's Soil Moisture and Ocean Salinity mission—Achievements and applications after more than 6 years in orbit. Special Issue: ESA's Soil Moisture and Ocean Salinity Mission - Achievements and Applications. *Remote Sensing of Environment*, *180*, 1–2.

Kerr, Y. H., Waldteufel, P., Wigneron, J.-P., Martinuzzi, J., Font, J., & Berger, M. (2001). Soil moisture retrieval from space: The soil moisture and ocean salinity (SMOS) mission. *IEEE Transactions on Geoscience and Remote Sensing*, *39*(8), 1729–1735.

Liou, K. N. (1980). *An introduction to atmospheric radiation*. Orlando, FL: Academic Press. 6.2.2, 184ff.

Mironov, V., Dobson, M., Kaupp, V., Komarov, S., & Kleshchenko, V. (2004a). Generalized refractive mixing dielectric model for moist soils. *IEEE Transactions on Geoscience and Remote Sensing*, *42*(4), 773–785.

Muñoz Sabater, J., de Rosnay, P., Albergel, C., & Isaksen, L. (2018). Sensitivity of soil moisture analyses to contrasting background and observation error scenarios. *MPDI Water*, *10*(7), 890.

Muñoz Sabater, J., Lawrence, H., Albergel, C., de Rosnay, P., Isaksen, L., Mecklenburg, S., et al. (2019). Assimilation of SMOS brightness temperatures in the ECMWF Integrated Forecasting System. *Quarterly Journal of the Royal Meteorological Society*, *2019*, 1–26. https://doi.org/10.1002/qj.3577

Njoku, E. G., & Entekhabi, D. (1996). Passive microwave remote sensing of soil moisture. *Journal of Hydrology*, *184*, 101–129.

Nkiaka, E., Nkiaka, N. R., & Nawaz, L. J. C. (2016). Evaluating global reanalysis precipitation datasets with rain gauge measurements in the Sudano-Sahel region: Case study of the Logone catchment, Lake Chad Basin. *Meteorological Applications*, *24*, 9–18. 2017, 2016 in Wiley Online Library,https://doi.org/10.1002/met.1600

Parrens, M., Calvet, J.-C., de Rosnay, P., & Decharme, B. (2014). Benchmarking of L-band soil microwave emission models. *Remote Sensing of Environment*, *140*, 407–419. https://doi.org/10.1016/j.rse.2013.09.017

Pellarin, T., Wigneron, J.-P., Calvet, J.-C., Berger, M., Douville, H., Ferrazzoli, P., et al. (2003). Two-year global simulation of L-band brightness temperatures over land. *IEEE Transactions on Geoscience and Remote Sensing*, *41*(9), 2135–2139.

Reichle, R. H., & Koster, R. D. (2004). Bias reduction in short records of satellite soil moisture. *Geophysical Research Letters*, *31*, L19510. https://doi.org/10.1029/2004GL020938

Sabater, J. M., de Rosnay, P., & Balsamo, G. (2011). Sensitivity of L-band NWP forward modeling to soil roughness. *International Journal of Remote Sensing*, *32*(19), 5607–5620. https://doi.org/10.1080/01431161.2010.507260

Tian, Y., Peters-Lidard, C. D., Harrison, K. W., You, Y., Ringerud, S., Kumar, S. V., & Turk, J. F. (2015). An examination of methods for estimating land surface microwave emissivity. *Journal of Geophysical Research: Atmospheres*, *120*, 11,114–11,128. https://doi.org/10.1002/2015JD023582

Tsang, L., Kong, J. A., & Shin, R. T. (1985). *Theory of microwave remote sensing*. Hoboken. New York: Wiley.

Wang, J., & Schmugge, T. (1980). An empirical model for the complex dielectric permittivity of soils as a function of water content. *IEEE Transactions on Geoscience and Remote Sensing*, *18*, 288–295.

Wigneron, J.-P., Kerr, Y., Waldteufel, P., Saleh, K., Escorihuela, M.-J., Richaume, P., et al. (2007). L-band Microwave Emission of the Biosphere (L-MEB) model: Description and calibration against experimental data sets over crop fields. *Remote Sensing of Environment*, *107*, 639–655.

Wilheit, T. T. (1978). Radiative transfer in a plane stratified dielectric. *IEEE Transactions on Geoscience and Remote Sensing*, *GE-16*, 138–143.